

Josu MAIORA, Manuel GRAÑA¹

A COMPUTER AIDED DIAGNOSTIC SYSTEM FOR SURVIVAL ANALYSIS AFTER EVAR TREATMENT OF AAA

Abdominal Aortic Aneurysm (AAA) is a local dilation of the Aorta that occurs between the renal and iliac arteries. Recently developed treatment involves the insertion of an endovascular prosthetic (EVAR), which has the advantage of being a minimally invasive procedure but also requires monitoring to analyze postoperative patient outcomes. The most widespread method for monitoring is computerized axial tomography (CAT) imaging, which allows 3D reconstructions and segmentations of the aorta's lumen of the patient under study. Previously published methods measure the deformation of the aorta between two studies of the same patient using image registration techniques. This paper applies neural network and statistical classifiers to build a predictor of patient survival. The features used for classification are the volume registration quality measures after each of the image registration steps. This system provides the medical team an additional decision support tool.

1. INTRODUCTION

Cardiovascular diseases, that involve heart and blood vessels, are the main causes of death in the western countries. Among these diseases, we have the Abdominal Aortic Aneurysms (AAA) that is a focal dilation of the aorta in the abdominal region. The use of the endovascular prostheses for aneurysm repair (EVAR) has proven to be an effective technique to reduce the pressure and rupture risk of aneurysms, offering shorter post-operation recovery than open surgical repair. The EVAR isolates the thrombosed vessel walls from the high pressure flow in the Aorta's lumen. When patient treatment has positive evolution, the thrombus sac between the EVAR and the vessel wall is reabsorbed after a time. EVAR evolution monitoring main instrument are Computerized Tomography (CT) images of the abdominal region after injection of an intravenous contrast agent. The main concern is that there may be leaks into or from the thrombus sac due to incorrect positioning, displacement or torsion of the EVAR graft, that is, liquid blood may appear inside the thrombus. This effect is called an endoleak and much current research efforts are devoted to detect it by image analysis procedures [8]. Fig. 1a is a typical slice of the CT volume, while Fig. 1b shows a sagittal view of the volume with the segmented aorta, stent graft and thrombus. Such images of the patient's abdominal area are available in the clinical routine as a set of 2D images whose visual analysis is time-consuming.

Most previous image processing methods related to the EVAR monitoring dealt with lumen and thrombus segmentation problems [11,13,18] and few addressed the lumen registration to estimate the deformation of the stent [4,10]. The aim of our work is to make an automatic analysis of the AAA, yielding visual and quantitative information for monitoring and tracking of patients who underwent EVAR, allowing classifying their evolution as favourable or unfavourable. In this paper we present a computer aided system for EVAR prognosis based on classification systems trained on the patient's data. Specifically, data features consist in the measurements of the deformation of the lumen between two different time instants [4,10] obtained as the image registration quality measures. Visual rendering of AAA and EVAR transformation data can help the physician to recognize deformation patterns having a high probability of dangerous progression of the EVAR and the aneurysm. The quantitative features for the classification systems are the values of similarity metrics obtained after rigid, affine and deformable registration of the aortic lumen. The proposed system has two phases: a pipeline of image registration processes and a classification system based on the image similarity metrics resulting from the image registration steps. Such approaches have proven to be effective in classification problems [1,5,14].

¹ Computational Intelligence Group, University of the Basque Country Donostia, San Sebastián

Statistical classifiers and more specifically Support Vector Machines (SVM) has become a standard tool for the development of computer aided diagnosis support systems from data [3]. The image registration of Abdominal Aortic Aneurysms (AAA) after treatment Endovascular Aneurysm Repair (EVAR) has already been presented in [9].



Figure 1. (a) Axial view of thrombus and lumen in a CT orthoslice using the contrast agents, blood in lumen is highlighted for a better view. (b) 3D view of segmented lumen+stent-graft and thrombus with a sagittal CT image faded in.

2. METHODS

First, the lumen is segmented using a 3D region growing algorithm. After that, the registration of the lumen extracted from two datasets of the same patient obtained at different moments in time is computed and then, we quantify the deformations of the lumen computing the similarity metrics between the reference and the registered dataset after each different registration refinement step: rigid, affine and deformable. Finally we classify them as favorable or unfavorable using a neural network. In the following, we proceed to describe each component of the system.

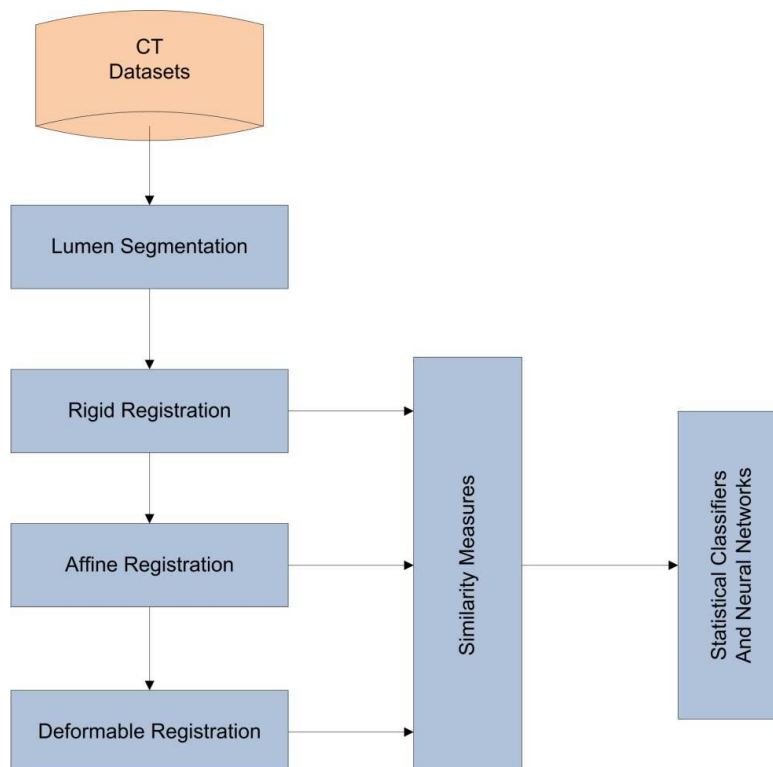


Figure 2. Pipeline of the classification input generation process.

2.1. REGION GROWING BASED LUMEN SEGMENTATION

Images obtained by Computerized Tomography (CT) are visualized as 3D volumes with appropriate software tools. Then, a segmentation process of lumen is performed. We have used a User-Guided Level Set Segmentation (UGLSS) [16] based on the well-known 3D active contour segmentation method called Region Competition [17] to get the Aorta lumen region in the images. During the preprocessing, probability maps are computed applying a smooth lower and upper threshold. This ensures that voxels inside the lumen have a positive value and the outside negative. After resampling the volume to get isotropic voxels of size (1,1,1), we define a ROI containing the lumen, and place a seed in it to initialize the evolving contour. We establish the parameters that control the propagation velocity and curvature velocity. An evolving contour is a closed surface $C(t,u,v)$ parametrized by variables u, v and by the time variable t . The contour evolves according to the following partial differential equation (PDE) driven with a F force, normal to the contour, \bar{N} :

$$\frac{\partial}{\partial t} C(t,u,v) = F \bar{N} \quad (1)$$

We compute the external force F by estimating the probability that a voxel belongs to the structure of interest and the probability that it belongs to the background at each voxel in the input image:

$$F = \alpha(P_{obj} - P_{bg}) + \beta k \quad (2)$$

where α and β are weights that modulate the relative contribution of the three components of F , and k is the mean curvature of the contour.

2.2. REGISTRATION

A sequence of three registration steps is performed; rigid, affine and deformable (B-splines) registrations. The first patient's study is considered the fixed reference image and the others are registered respect to it. A linear image intensity interpolator, Mutual Information metric and Regular Step Gradient Descent Optimizer are used. Rigid, affine and deformable registrations of the lumen provide a visual assessment of the evolution of the stent-graft. Figure 2 shows the progressive refinement of the matching between two Aorta lumen regions (red and blue) along the image registration pipeline.

2.2.1. RIGID REGISTRATION

First the two binary images corresponding to the patient lumen are roughly aligned by using a transform initialization and then the two images are registered using a rigid transformation. In three dimensions we have 6 degrees of freedom which can be defined as translation in the x,y and z directions, and rotations a, b and g about these three axes. From these unknowns we can construct a rigid body transformation matrix T_{rigid} . This transformation can be presented as a rotation R followed by a translation t that can be applied to any point x :

$$T_{rigid}(x) = Rx + t \quad (3)$$

2.2.2. AFFINE REGISTRATION

The rigid transformation is used to initialize a registration with an affine transform of the lumen. While a rigid transformation preserves the distances between all points in the object transformed, an affine transformation preserves parallel lines. This model has 12 degrees of freedom and allows for scaling and shearing:

$$T(x, y, z) = \begin{pmatrix} x \\ y \\ z \\ 1 \end{pmatrix} = \begin{pmatrix} a_{00} & a_{01} & a_{02} & a_{03} \\ a_{10} & a_{11} & a_{12} & a_{13} \\ a_{20} & a_{21} & a_{22} & a_{23} \\ 0 & 0 & 0 & 1 \end{pmatrix} \begin{pmatrix} x \\ y \\ z \\ 1 \end{pmatrix} \quad (4)$$

2.2.3. DEFORMABLE REGISTRATION

Finally, the deformable registration is computed in two steps, one at coarse resolution and secondly at fine resolution. The transform resulting from the affine registration is used as the bulk transform of a B-spline deformable transform. Free Form Deformations (FFDs) based in locally controlled functions such as B-splines are a powerful tool for modeling 3D deformable objects. We use FFDs to deform the lumen by manipulating an underlying mesh of control points. The resulting deformation controls the shape of the lumen and produces a smooth and continuous transformation. A spline based FFD is defined on the image domain:

$$\Omega = (x, y, z) \ 0 \leq x < X, 0 \leq y < Y, 0 \leq z < Z \quad (5)$$

where Φ denotes an $n_x \times n_y \times n_z$ mesh of control points with uniform spacing δ . In this case, the displacement field u defined by FFD can be expressed as the 3D tensor product of the familiar 1D cubic B-splines:

$$u(x, y, z) = \sum_{l=0}^3 \sum_{m=0}^3 \sum_{n=0}^3 \Theta_l(u) \Theta_m(v) \Theta_n(w) \Phi_{(l+m+n)} \quad (6)$$

where:

$$i = \left\lfloor \frac{x}{\delta} \right\rfloor - 1, j = \left\lfloor \frac{y}{\delta} \right\rfloor - 1, k = \left\lfloor \frac{z}{\delta} \right\rfloor - 1, u = \frac{x}{\delta} - \left\lfloor \frac{x}{\delta} \right\rfloor, v = \frac{y}{\delta} - \left\lfloor \frac{y}{\delta} \right\rfloor, w = \frac{z}{\delta} - \left\lfloor \frac{z}{\delta} \right\rfloor$$

and Θ_l represents the l -th basis function of the b-splines:

$$\begin{aligned} \Theta_1(s) &= (1-s)^3 6(s) \\ \Theta_2(s) &= (3s^2 - 6s^2 + 4) 6 \\ \Theta_3(s) &= (-3s^2 + 3s^2 + 3s + 1) 6 \\ \Theta_4(s) &= s^3 6 \end{aligned} \quad (7)$$

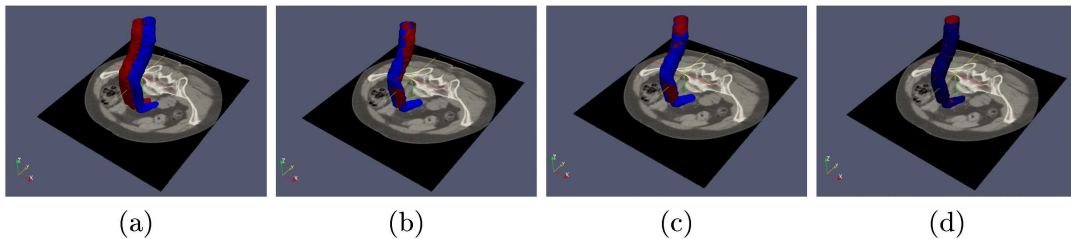


Figure 3. Visualization of fixed and moving images of the lumen: (a) before registration, (b) after rigid, (c) affine, and (d) deformable registration.

2.2.4. SIMILARITY METRICS

We compute two similarity metrics: the sum of squared intensity differences (SSD) and mutual information (MI) [15]. These similarity metrics have each been used widely in the past for nonrigid registration, to measure the intensity agreement between a deforming image and the target image. We briefly describe both distances in this section.

SSD is suitable when the images have been acquired through similar sensors and thus are expected to present the same intensity range and distribution. For voxel locations x_A in image A , within an overlap domain $\Omega_{A,B}^T$, comprising N voxels:

$$SSD = \frac{1}{N} \sum_{x_A \in \Omega_{A,B}^T} |A(x_A) - B^T(x_A)|^2 \quad (8)$$

Mutual information is a measure of how much information one random variable has about another. The information contributed by the images is simply the entropy of the portion of the image that overlaps with the other image volume, and the mutual information is a measure of the joint entropy respect to the marginal entropies:

$$I(A,B) = H(A) + H(B) - H(A,B) \quad (9)$$

where $I(A,B)$ is the mutual information, $H(A)$ and $H(B)$ are the marginal entropies of the fixed and moving images, and $H(A,B)$ is the joint entropy. We have computed the mean squares and mutual information similarity metrics for the evaluation of the registration in 3 registration processes, each of them with rigid, affine, deformable coarse and deformable fine methods. A decrease of both metric is observed in the consequent registration methods.

2.3. STATISTICAL CLASSIFICATION ALGORITHMS AND NEURAL NETWORKS

We deal with two class classification problem, given a collection of training/testing input feature vectors $X = \{\mathbf{x}_i \in \mathbb{R}^n, i = 1, \dots, l\}$ and the corresponding labels $\{y_i \in \{-1,1\}, i = 1, \dots, l\}$, which sometimes can be better denoted in aggregated form as a binary vector $\mathbf{y} \in \{-1,1\}^l$. We perform the classification in the Weka environment [6].

2.3.1. SUPPORT VECTOR MACHINES

The Support Vector Machine (SVM) [12] constructs a hyperplane or set of hyperplanes in a high- or infinite- dimensional space, which can be used for classification. Intuitively, a good separation is achieved by the hyperplane that has the largest distance to the nearest training data points of any class, since in general the larger the margin the lower the generalization error of the classifier. The approach to build a classifier system from the given data consists in solving the following optimization problem:

$$\min_{\mathbf{w}, b, \xi} \frac{1}{2} \mathbf{w}^T \mathbf{w} + C \sum_{i=1}^l \xi_i \quad (10)$$

subject to:

$$y_i(\mathbf{w}^T \phi(\mathbf{x}_i) + b) \geq (1 - \xi_i), \quad \xi_i \geq 0, \quad i = 1, 2, \dots, n. \quad (11)$$

where \mathbf{w} is the normal vector to the hyperplane, C is a constant and ξ_i , measures the degree of misclassification of the datum \mathbf{x}_i . We build the SVM classifier, testing both with a linear kernel and

Radial Basis Function (RBF) kernel. In both cases we fix the parameter value $C = 1$, and we fix the RBF width parameter $\gamma = 0.1$.

2.3.2. BACKPROPAGATION

Backward propagation of errors, or backpropagation (BP), [12,7] is a non-linear generalization of the squared error gradient descent learning rule for updating the weights of artificial neurons in a single-layer perceptron, to multi-layer feed-forward networks, also called Multi-Layer Perceptron (MLP). The backpropagation of the error allows to compute the gradient of the error function relative to the hidden units' weights. During on-line learning, the weights of the network are updated at each input data item presentation. We have used the resilient backpropagation, which uses only the derivative sign to perform the weight updating. We restrict our presentation of BP to train the weights of the MLP for a two class problem. Let the instantaneous error E_p be defined as:

$$E_p(\mathbf{w}) = \frac{1}{2} (y_p - z_K(\mathbf{x}_p))^2 \quad (12)$$

where y_p is the p -th desired output y_p , and $z_K(x_p)$ is the network output when the p -th training exemplar x_p is inputted to the MLP composed of K layers, whose weights are aggregated in the vector \mathbf{w} . We use neuron units with sigmoid transfer function trained to minimize the mean squared error function using Levenberg-Marquardt optimization, with a minimum performance gradient of 1e-10. It consists in solving the equation:

$$(J^T J + I)d = J^T E \quad (13)$$

where J is the Jacobian matrix that contains first derivatives of the network errors with respect to the weights and biases, and E is the error vector containing the output errors for each input vector used on training the network. In the computational experiments, we have found empirically that *(number of features + number of classes)/2* hidden units are appropriate to find excellent classification and generalization results. The learning rate value is fixed to 0.1.

2.3.3. RANDOM FOREST

This classifier is a multi-classifier based on Random Trees. This classifiers are a specific variation of a decision tree [2]. When the tree is constructed and trained, each node contains a discriminant criteria which allows to decide how to go down or traverse the tree. The classifier is able to detect key-point occurrences even in the presence of image noise, variations in scale, orientation and illumination changes. A Random Tree is called random because instead of performing exhaustive search in order to find the best combination of features to define a discriminant criteria in each node, just some random combinations of them are evaluated. When the number of different classes to be recognized and the size of the descriptor of such classes is high, an exhaustive analysis is not feasible. Additionally, the examples to be used for the training process are selected at random from the available ones. The combination of several random trees forms a multi-classifier known as Random Forest (RF). One of the advantages of the Random Forest is its combinational behavior. If a random tree can be weak itself, i.e. its recognition rate is low, then the combination of such weak tree can generate a strong classifier. We build the RF classifier with 20 trees each of depth 5. Variations of these parameters around these values do not cause significant changes in final results.

3. RESULTS

We have tested the approach with 15 datasets corresponding to 5 patients which have been subjected to EVAR with stent-graft devices. Each dataset is comprised between 300 and 500 axial slices

that form a three dimensional image. The CT datasets were obtained from a LightSpeed16 CT scanner (GE Medical Systems, Fairfield, CT, USA) with $512 \times 512 \times 354$ voxel resolution and $0.725 \times 0.725 \times 0.8$ mm. spatial resolution. The time elapsed between different studies of the same subject varies between 6 and 12 months. Four datasets, corresponding to one patient, are validated by the doctors as having a favorable evolution and 11, corresponding to the remaining 4 patients, as unfavorable, according to aneurysm volume and surface measures, as well as blood leakages in the aneurysm sac.

Input feature vectors are eight-dimensional. Four features correspond to the MSD metric values, the other four to the MI metric values. Metric values are computed after each registration step between each pair segmented lumens.

We train over the set of features different classifiers and we show the results for accuracy, sensitivity, specificity, and area under the ROC (AUC). Table 1 gives average results from on a one-leave-out cross-validation strategy on this database. We obtain the best results for linear SVM, followed by Random-Forest and MLP-BP, while RBF-SVM gives us the less accurate results. This can be explained by the great unbalance of the sample data classes. Results are promising of high accuracy prognosis, needing confirmation on a larger patient population.

Table 1. Cross-validation results over the similarity metric features computed from the CT datasets for EVAR evolution classification.

Classifier	Accuracy	Sensitivity	Specificity	AUC
Linear SVM	0.72	0.75	0.67	0.97
RBF SVM	0.77	0.80	0.70	0.98
BP- MLP	0.73	0.71	0.80	0.97
Random-Forest	0.91	0.99	0.73	0.99

4. CONCLUSIONS

Building Computer Aided Diagnosis systems for the prognosis of EVAR applied to AAA has not previously dealt with in the literature. Therefore, the whole feature extraction and classification pipeline presented in this paper is the only instance of such approach up to now. The process pipeline is as follows: After segmentation of the Aorta's lumen, a registration process is carried out over binary images improving on the works that perform registration over point sets, which always involve a greater loss of information. Registering images from different imaging datasets obtained from the same patient at different times provide us quantitative information about deformation of the stent-graft.

The feature vectors consist of the similarity measures computed on the segmented lumen after rigid, affine and deformable registration. The datasets of the patients have been previously validated by the medical team as having a favorable or unfavorable evolution.

Considering the average accuracy data achieved by most of the classifiers tested, our main conclusion is that the proposed feature extraction is very effective in providing a good discrimination between patients that can easily be exploited to build classifier systems predicting the evolution of other patients and provide support for the physician decision making. Further ongoing works with a more extensive database are aimed to confirm these conclusions.

5. ACKNOWLEDGMENTS

Experimental data has been provided by the Hospital Donostia.

BIBLIOGRAPHY

- [1] ABRAHAM A., et al., Hybrid learning machines., Neurocomputing, Vol. 72, No. 13-15, 2009, pp. 2729-2730.
- [2] BREIMAN L., et al., Random forests, Machine learning, Vol. 45, No. 1, 2001, pp. 5-32.

- [3] BURGESS C.J., et al., A tutorial on support vector machines for pattern recognition, *Data mining and knowledge discovery*, Vol. 2, No. 2, 1998, pp. 121–167.
- [4] DEMIRCI S., et al., *Quantification of Abdominal Aortic Deformation after EVAR*, SPIE Medical Imaging, Orlando, Florida, USA, 2009.
- [5] DERRAC J., et al., A First Study on the Use of Coevolutionary Algorithms for Instance and Feature Selection, *Hybrid Artificial Intelligence Systems*, 2010, pp. 557–564.
- [6] HALL M., et al., The WEKA data mining software, *ACM SIGKDD Explorations Newsletter*, Vol. 11, 2009, pp. 10.
- [7] HAYKIN S., et al., *Neural Networks: A comprehensive foundation*, Prentice Hall 1999.
- [8] MACIA I., et al., Detection of type II endoleaks in abdominal aortic aneurysms after endovascular repair, *Computers in Biology and Medicine*, 2011.
- [9] MAIORA J., et al., Thrombus Change Detection After Endovascular Abdominal Aortic Aneurysm Repair, *International Journal of Computer Assisted Radiology and Surgery*, Heidelberg, Vol. 5, Suppl. 1, 2010, pp. S15.
- [10] MATTES J., et al., Quantification of the migration and deformation of abdominal aortic aneurysm stent grafts, *Medical Imaging 2006: Image Processing*, Vol. 6144, 2006, pp. 61440V.
- [11] OLABARRIAGA S.D., et al., Segmentation of thrombus in abdominal aortic aneurysms from CTA with nonparametric statistical grey level appearance modelling, *IEEE Transactions On Medical Imaging*, Vol. 24, No. 4, 2005, pp. 477-485.
- [12] RUMELHART D.E., et al., Learning representations by backpropagating errors, *Nature*, 1986, pp. 533–536.
- [13] SUBASIC M., et al., Region-based deformable model for aortic wall segmentation, In: *Proc. 3rd Int. Symp. Image and Signal Processing and Analysis ISPA 2003*, Vol. 2, 2003, pp. 731–735.
- [14] WOZNIAK M., et al., Designing fusers on the basis of discriminants–evolutionary and neural methods of training, *Hybrid Artificial Intelligence Systems*, 2010, pp. 590–597.
- [15] YANOVSKY I., et al., Comparing registration methods for mapping brain change using tensor-based morphometry, *Medical Image Analysis*, Vol. 13, No. 5, 2009, pp. 679-700.
- [16] YUSHKEVICH P.A., et al., User-guided 3D active contour segmentation of anatomical structures: significantly improved efficiency and reliability, *Neuroimage*, Vol. 31, No. 3, 2006, pp. 1116–1128.
- [17] ZHU, S.C., et al., Region competition: Unifying snakes, region growing, and Bayes/MDL for multiband image segmentation, *IEEE Transactions On Pattern Analysis And Machine Intelligence*, Vol. 18, No. 9, 1996, pp. 884-900.
- [18] ZHUGE F., et al., An abdominal aortic aneurysm segmentation method: Level set with region and statistical information, *Medical Physics*, Vol. 33, No. 5, 2006, pp. 1440-1453.